Geophys. J. R. astr. Soc. (1983) 72, 461–481

Regional dispersion of first-order overtone Rayleigh waves

Emile A. Okal and Bong-Gon Jo *Department of Geology and Geophysics, Yale University, Box 6666, New Haven, Connecticut 06511, USA*

Received 1982 August 9; in original form 1982 April 20

Summary. Records of the first Rayleigh overtone in the 70–110 s period range, following deep subduction zone events, are analysed through standard surface wave techniques to retrieve dispersion characteristics. In the oceanic environment, our data are in general agreement with published models obtained from regionalization of fundamental Rayleigh wave paths. A general increase in phase velocity with age is observed, with a somewhat smaller effect on group velocities. Continental and trench area data are processed through a regionalization scheme, indicating that the difference between average continental and oceanic velocities (both phase and group) is about 0.2 km s^{-1} at periods of the order of 95 s. An investigation of a set of simple models, allowing structural heterogeneities between oceans and continents down to variable depth, suggests that they probably do not extend past the bottom of the asthenosphere (250 km).

1 Introduction

Substantial lateral heterogeneities, in particular differentiating between continental and oceanic structures, are known to exist in the Earth's crust and upper mantle. However, the important question of their depth extent is still being debated and the consequences of the final answer to this problem will be far-reaching: strong lateral heterogeneity at depth, interpreted in the framework of additional data from geochemical studies (De Paolo 1981), could require chemical differentiation, which in turn would constrain convection in the mantle to its shallowest layers.

Most of our knowledge of structural lateral heterogeneity has come from seismic studies. Using regionalization of long-period surface waves, Toksöz & Anderson (1966) first obtained different dispersion curves for three geological provinces: shields, tectonic continents and oceans. Their method was extended and refined, notably by Kanamori (1970), Dziewonski (1970) and Knopoff (1972). Meanwhile, progress in marine geophysics showed that the ageing of the oceanic lithosphere was accompanied by structural changes (Tréhu, Sclater & Nabelek 1976) leading to a variation with age of the seismic structure of oceanic areas (Leeds, Kausel & Knopoff 1974; Mitchell & Yu 1980). Okal (1977, hereafter Paper I) showed that the incorporation of this intrinsic oceanic heterogeneity in regionalization

schemes reduces the need for deep lateral heterogeneities between oceans and continents, which he was able to constrain to the upper 250 km of the Earth's structure. Similar conclusions were also reached by Nakanishi (1981).

Seismic body wave studies of lateral heterogeneities have been of two kinds: *P*-wave residual investigations (e.g. Poupinet 1979; Romanowicz 1979, 1980), and multiple *ScS* studies, allowing in principle investigation of areas where no seismic stations are available (e.g. deserts and oceans). The latter have been controversial, Okal & Anderson (1975) showing that they can explain their observations by constraining major continent versus ocean heterogeneities to the top 250 km, while Sipkin & Jordan (1976, 1980) have claimed the need to extend them at least 400, and possibly 600 km. Jordan (1975) has sketched tentative *S*-wave profiles of continental and oceanic structure with heterogeneity carried down to about 675 km, and reviewed (Jordan 1979) other efforts in the matter.

The resolving power of fundamental surface waves in the search for deep structures is directly linked to their frequency, and such investigations require the use of ultra-long periods, typically in the range of 300 s for depths on the order of 300–500 km. It becomes difficult to work with such datasets, because of their relative paucity, and of the problems associated with regionalization at very long wavelengths. Additionally, the interpretation of body wave data is itself made very difficult and non-unique at these depths. In order to extend our insight into deep lateral structure, several avenues are available: one can, following Jordan (1978) and Silver & Jordan (1981), push for still longer periods, searching systematically for variations in observed eigenfrequencies of the Earth's normal modes.

Another possibility is to investigate regional dispersion of overtone surface waves. Because their eigenfunctions sample the Earth deeper than their fundamental counterparts, overtones are sensitive to deep structure in a range of frequencies higher (and therefore more accessible) than fundamentals. As opposed to Love overtones, whose group velocities are very similar to those of the fundamentals, Rayleigh overtones travel faster, and can be well separated on seismograms. In a short paper (Okal 1979a), we reported such recordings of first Rayleigh overtones ($_1R$) as individual seismic phases following large deep earthquakes in subduction zones, and showed that standard surface-wave processing techniques could be successfully applied to these waves. Additionally, Cara (1978) used spatial filtering techniques to extract smaller Rayleigh overtones from shallower events, and conducted inversions of *S*-wave velocity structure in the Pacific Ocean and North America. His results did not require deep lateral heterogeneity.

Additionally, any regionalization of the Earth can be carried out in two ways: either by constraining *a priori* the boundaries of the provinces to correlate with known large-scale tectonic features (a traditional approach, e.g. Kanamori 1970; Paper I; Jordan 1981), or by decomposing the lateral heterogeneity on to spherical harmonics. Following this approach, Nakanishi & Anderson (1981) have regionalized fundamental group velocity data between 100 and 300 s, and inverted these data into a spherical harmonics expansion of lateral heterogeneity. More recently, Masters *et al.* (1982) have explored the P_2^0 component of the Earth's lateral heterogeneity using a large dataset of fundamental spheroidal mode frequencies, and found that its most significant term does not correlate with oceans and continents, but rather may involve important structural differences between old oceans and slab on the one hand, and the fast spreading ridges, such as the East Pacific Rise, on the other. These findings, which stress the importance of intrinsic oceanic heterogeneity are also in the line of such recent studies as Montagner & Jobert's (1981), who have documented a downward expansion of the asthenospheric channel in the vicinity of the East Pacific Rise.

This paper presents a study of $_1R$ dispersion as obtained from high-quality records of

individual phases of Rayleigh overtones from a number of deep earthquakes. After presenting the dataset, we study the theoretical structure of the ${}_1R$ wave at the surface of the Earth, and use these results to discuss the isolation of ${}_1R$, notably from the second overtone, ${}_2R$. We then proceed to measure phase and group velocities along selected paths, compare our results to values suggested by published models in oceanic environments and regionalize our group velocity values involving continental paths. A discussion of our results and a comparison with various theoretical models suggest a maximum depth of 250 km for large-scale heterogeneity in the mantle.

2 Dataset

For the purpose of this study, we shall isolate high-quality records of ${}_1R$ Rayleigh overtones in the range 70–110 s, which can be studied as individual seismic phases. Examples of the data, including one given by Okal (1979a), are reproduced in Fig. 1. Theoretical investigations of normal mode excitation coefficients show that the first Rayleigh overtone is adequately excited in the 80 s period range by large ($M_0 \geq 10^{27}$ dyne cm) events at the bottom of subduction zones, as well as by larger ($M_0 = 10^{28}$ dyne cm) earthquakes at intermediate depths, on the order of 100–150 km. Although we occasionally identified multiple passages of ${}_1R$ (the so-called ${}_1R_2$ or ${}_1R_3$ phases), we avoid using these records in phase velocity studies, since their paths will often involve the difficult choice of a large unknown integer in the variation of the spectral phase, as well as a maximum deviation from 'pure-path' behaviour; thus we will concentrate on the first passage of the first Rayleigh overtone (${}_1R_1$). Table 1 is a list of records used in this study, with pertinent epicentral information. Most of the data consist of long-period vertical WWSSN records from three deep subduction zone events: the Japan Sea earthquake of 1973 September 29, the Izu–Bonin subduction zone earthquake of 1978 March 7, and the Argentine earthquake of 1977 October 22. All these events have focal mechanisms involving nearly pure dip-slip on a vertical fault (Furumoto & Fukao 1976; Koyama 1978; Okal 1979b; Masters & Gilbert 1979), with

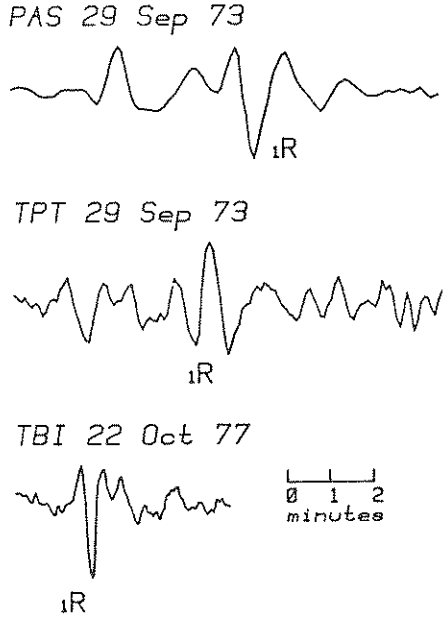

Figure 1. Examples of seismograms of ${}_1R$ wavetrains used in this study.

Table 1. (a) Earthquakes used in this study.

Event	Date	Origin Time GMT	Epicenter (°N)	(°E)	Depth (km)	Magnitude (mb)	Moment (dyn-cm)
1	29 Sep 73	00:44:01	41.93	130.99	575	6.3	$7\ 10^{27}$
2	7 Mar 78	02:48:47	31.99	137.61	430	6.5	$7\ 10^{26}$
3	22 Oct 77	17:57:15	-27.96	-62.82	590	6.2	$5\ 10^{26}$
4	29 Jun 73	10:37:40	38.79	130.09	549	6.1	
5	10 Sep 73	07:43:32	42.48	131.05	552	5.8	$1.4\ 10^{26}$
6	6 Dec 78	14:02:04	44.55	146.67	115	6.3	$3\ 10^{27}$

Table 1. (b) Seismic records used in this study.

Event	Station Code	and Name	Instrument	Distance (°)	Azimuth from source (°)
1	AAE	Addis-Ababa, Ethiopia ($_1R_2$)	WWSSN	274.51	98.3
1	ARE	Arequipa, Peru	WWSSN	148.15	43.4
1	GRM	Grahamstown, South Africa	WWSSN	121.30	251.9
1	LUB	Lubbock, Texas	WWSSN	90.53	41.5
1	NAI	Nairobi, Kenya ($_1R_2$)	WWSSN	266.22	92.0
1	OBN	Obninsk, USSR	K-P-Tcha 100	59.08	318.3
1	PAS	Pasadena, California	ULP "33"	81.28	51.4
1	PPT	Papeete, Tahiti, Fr. Polynesia	LDG Broad-band	94.09	109.7
1	TPT	Tiputa, Rangiroa, Fr. Polynesia	LDG Broad-band	93.68	106.6
1	WEL	Wellington, New Zealand	WWSSN	91.86	148.4
2	AAE	Addis-Ababa, Ethiopia	WWSSN	92.65	282.5
2	AAM	Ann Arbor, Michigan	WWSSN	29.76	29.4
2	BDF	Brasilia, Brazil ($_1R_2$)	IDA	196.91	198.1
2	COL	College Station, Alaska	WWSSN	54.96	30.1
2	COR	Corvallis, Oregon	WWSSN	74.06	47.1
2	DAL	Dallas, Texas	WWSSN	97.45	43.5
2	LON	Longmire, Washington	WWSSN	73.90	44.6
2	LPA	La Plata, Argentina	WWSSN	166.72	105.4
2	LPB	La Paz, Bolivia	WWSSN	152.05	62.0
2	MSO	Missoula, Montana	WWSSN	78.42	41.6
2	NAI	Nairobi, Kenya	WWSSN	99.84	274.9
2	PAS	Pasadena, California	ULP "33"	82.92	54.0
2	PPT	Papeete, Tahiti, Fr. Polynesia	LDG Broad-band	85.40	113.7
2	SHA	Spring Hill, Alabama	WWSSN	103.93	39.4
2	SUR	Sutherland, South Africa ($_1R_2$)	IDA	232.90	71.9
2	WEL	Wellington, New Zealand	WWSSN	80.72	152.5
3	AAE	Addis-Ababa, Ethiopia	WWSSN	104.55	87.6
3	AFI	Afiamalu, Western Samoa	WWSSN	98.44	248.6
3	ATU	Athens, Greece	WWSSN	104.33	54.7
3	BEC	Hamilton, Bermuda	WWSSN	60.23	358.4
3	CTA	Charter Towers, Australia	WWSSN	124.33	213.7
3	GRM	Grahamstown, South Africa	WWSSN	74.81	120.0
3	KAB	Kabul, Afghanistan	WWSSN	138.67	69.0
3	KEV	Kevo, Finland	WWSSN	116.05	32.9
3	NAI	Nairobi, Kenya	WWSSN	98.05	95.8
3	NDI	New Delhi, India	WWSSN	145.10	79.7
3	QUE	Quetta, Pakistan	WWSSN	136.53	75.0
3	SHI	Shiraz, Iran	WWSSN	124.18	72.0
3	TAB	Tabriz, Iran	WWSSN	121.24	60.8
3	TAU	Hobart, Tasmania, Australia	WWSSN	103.96	202.5
3	TBI	Tubuai, French Polynesia	LDG Broad-band	76.40	250.5
3	WIN	Windhoek, Namibia	WWSSN	71.36	106.2
4	PPT	Papeete, Tahiti, Fr. Polynesia	LDG Broad-band	93.62	109.4
4	TPT	Tiputa, Rangiroa, Fr. Polynesia	LDG Broad-band	93.44	106.2
5	PPT	Papeete, Tahiti, Fr. Polynesia	LDG Broad-band	94.30	109.7
6	TPT	Tiputa, Rangiroa, Fr. Polynesia	LDG Broad-band	84.08	117.5
6	RKT	Rikitea, Gambier, Fr. Polynesia	LDG Broad-band	98.14	114.2

moments varying between 5×10^{26} and 7×10^{27} dyne cm. We supplement this dataset with records obtained on the broad-band instruments of the French Polynesian network, from a few more deep Japanese earthquakes and from the intermediate depth 1978 December 6, Kuriles event. We also include in the dataset two records of the phase $_1R_2$ from the 1978 Izu event, at the IDA stations BDF and SUR, which we process for group velocity only, at much longer periods.

Fig. 2 presents maps of the paths along which phase and group velocity measurements were taken, for the three main events. Each box is an equidistant azimuthal projection centred on the epicentre or its antipodes. Focal mechanisms are also sketched. For the simple mechanism involved in events 1, 2 and 3, the radiation pattern is two-lobed for all Rayleigh overtones and at all frequencies and depths (e.g. Kanamori & Cipar 1974).

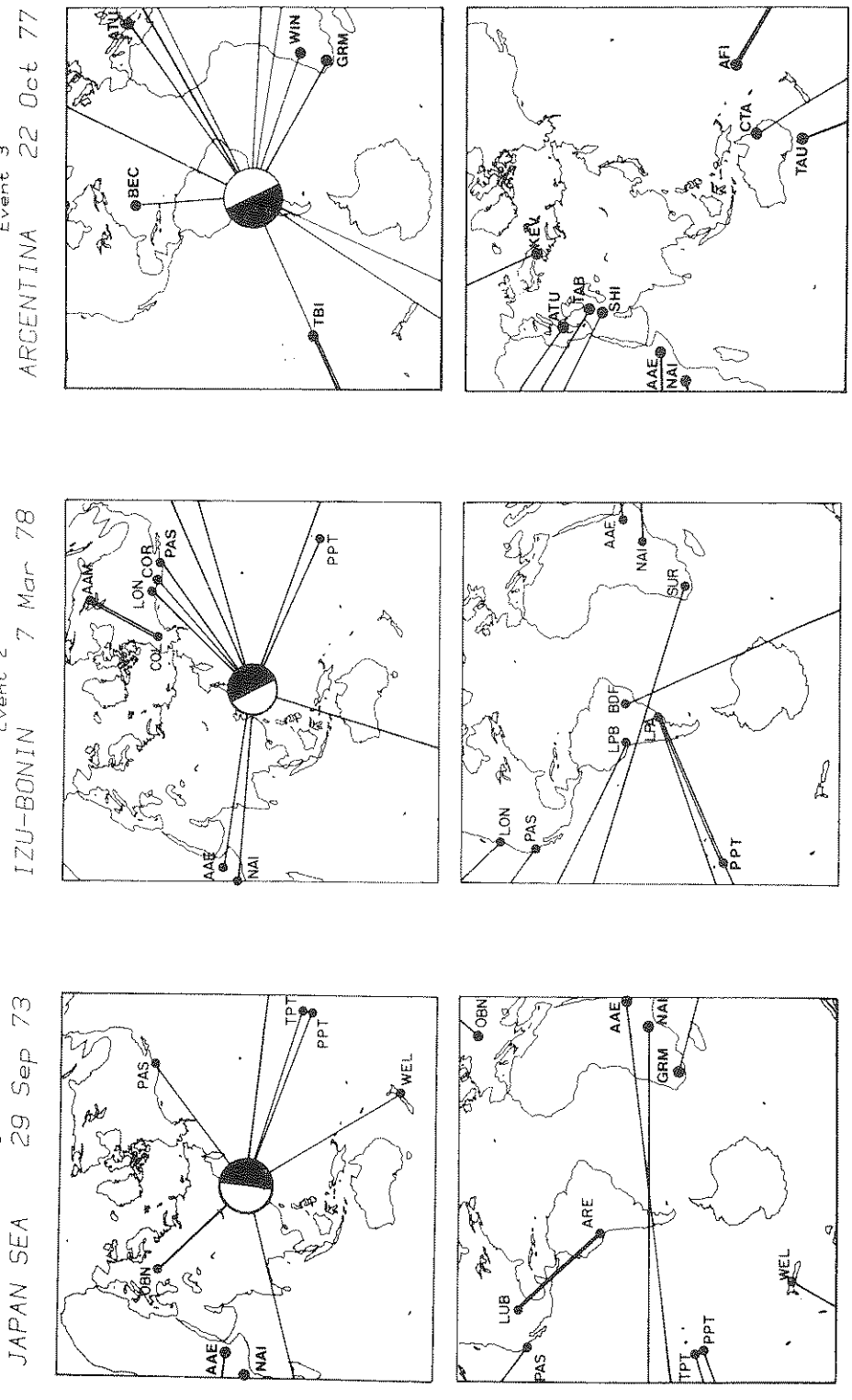

Figure 2. Map of the paths used in the phase and group velocity investigations for the three main subduction zone events. For each earthquake, the two maps are equidistant azimuthal projections centred respectively on the epicentre and its antipodes. Single lines show group velocity paths, double lines paths used in phase velocity two-station studies. For clarity, the stations involved in the spatial filtering phase velocity study have been omitted. Focal mechanisms are also sketched.

3 Structure of the first Rayleigh overtone wave ${}_1R$

Before processing any of the data described above, it is important to make sure that they are indeed the first Rayleigh overtone, and in particular are not being contaminated by the second overtone ${}_2R$, known to be travelling at a group velocity only slightly higher than that of ${}_1R$ at the high-frequency end of our range of interest (see for example Cara 1978).

One way of doing so is to study the complex spectral ratio of the seismic displacements along the vertical and radial (away from the source) axes, and to compare them with their theoretical values. For this purpose, we use records of the 1973 event (the largest among the deep events investigated) at Papeete, Tahiti, in a direction where Love wave contamination

Table 2. Theoretical aspect ratios of ${}_0R$, ${}_1R$ and ${}_2R$.

Mode	Period (s)	$\chi_3 = u_x/u_z$ (*)	Mode	Period (s)	$\chi_3 = u_x/u_z$ (*)
	MODEL 1066A			HOMOGENEOUS EARTH MODEL	
${}_0S_{89}$	106.26	-0.656	${}_0S_{75}$	100.75	-0.662
${}_0S_{100}$	95.16	-0.662	${}_0S_{100}$	76.08	-0.667
${}_0S_{122}$	78.52	-0.671	${}_0S_{125}$	61.12	-0.670
${}_0S_{154}$	62.39	-0.680	${}_0S_{150}$	51.08	-0.671
${}_0S_{184}$	52.21	-0.685	${}_0S_{175}$	43.87	-0.673
${}_0S_{212}$	45.26	-0.689	${}_0S_{200}$	38.45	-0.674
${}_0S_{239}$	40.09	-0.691	${}_0S_{225}$	34.22	-0.675
${}_0S_{266}$	35.97	-0.693	${}_0S_{250}$	30.82	-0.675
${}_0S_{293}$	32.61	-0.694	${}_0S_{275}$	28.04	-0.676
${}_0S_{320}$	29.81	-0.695	${}_0S_{300}$	25.72	-0.676
${}_1S_{61}$	108.27	-0.088	${}_1S_{50}$	118.75	-0.391
${}_1S_{86}$	83.25	-0.301	${}_1S_{75}$	82.88	-0.457
${}_1S_{90}$	80.31	-0.323	${}_1S_{100}$	63.78	-0.491
${}_1S_{100}$	73.84	-0.369	${}_1S_{125}$	51.88	-0.511
${}_1S_{118}$	64.53	-0.429	${}_1S_{150}$	43.75	-0.525
${}_1S_{149}$	53.09	-0.495	${}_1S_{175}$	37.84	-0.535
${}_1S_{176}$	46.01	-0.532	${}_1S_{200}$	33.34	-0.542
${}_1S_{204}$	40.41	-0.559	${}_1S_{225}$	29.80	-0.549
${}_1S_{232}$	36.01	-0.577	${}_1S_{250}$	26.94	-0.554
${}_1S_{259}$	32.57	-0.591	${}_1S_{275}$	24.59	-0.558
${}_1S_{286}$	29.73	-0.601			
${}_1S_{313}$	27.33	-0.609			
${}_2S_{50}$	108.05	0.936	${}_2S_{50}$	101.42	-0.033
${}_2S_{75}$	79.60	0.236	${}_2S_{75}$	73.11	-0.237
${}_2S_{101}$	64.25	-0.101	${}_2S_{100}$	57.38	-0.327
${}_2S_{130}$	53.25	-0.279	${}_2S_{125}$	45.63	-0.315
${}_2S_{157}$	45.94	-0.369	${}_2S_{150}$	39.00	-0.360
${}_2S_{184}$	40.42	-0.427	${}_2S_{175}$	34.08	-0.392
${}_2S_{213}$	35.82	-0.471	${}_2S_{200}$	30.28	-0.416
${}_2S_{239}$	32.52	-0.500	${}_2S_{225}$	27.25	-0.435
${}_2S_{266}$	29.69	-0.523	${}_2S_{250}$	24.78	-0.449
${}_2S_{293}$	27.31	-0.541	${}_2S_{275}$	22.72	-0.462

* Taken as positive for prograde motion.

on the horizontal instruments is minimal, due to the focal radiation pattern, shown on Fig. 2.

As opposed to fundamental Rayleigh waves, for which the simple theory of a homogeneous Poisson solid half-space predicts a (horizontal to vertical) aspect ratio $u_x/u_z = 0.681$, there is no simple way of finding the aspect ratio of an overtone Rayleigh wave, whose mere existence requires either radial heterogeneity or sphericity. For this purpose, we have investigated the theoretical aspect ratio of ${}_0R$, ${}_1R$ and ${}_2R$, for both a homogeneous Poisson sphere, and Gilbert & Dziewonski's (1975) model 1066A. As shown in Table 2, these are found to be significantly model dependent, and in the case of structures involving layering, such as 1066A, also frequency dependent. Furthermore, comparable values of the aspect ratio are predicted for ${}_1R$ and ${}_2R$ for periods less than 55 s. Thus, the use of the aspect ratio alone is not sufficient to assess the possible contamination of ${}_1R$. The spectral phase information, however, can discriminate between a pure overtone wave, and a contaminated one. All Rayleigh-type surface waves, overtones as well as fundamentals, are expected to have an absolute 90° phase lag between their vertical and radial components (although the sign of

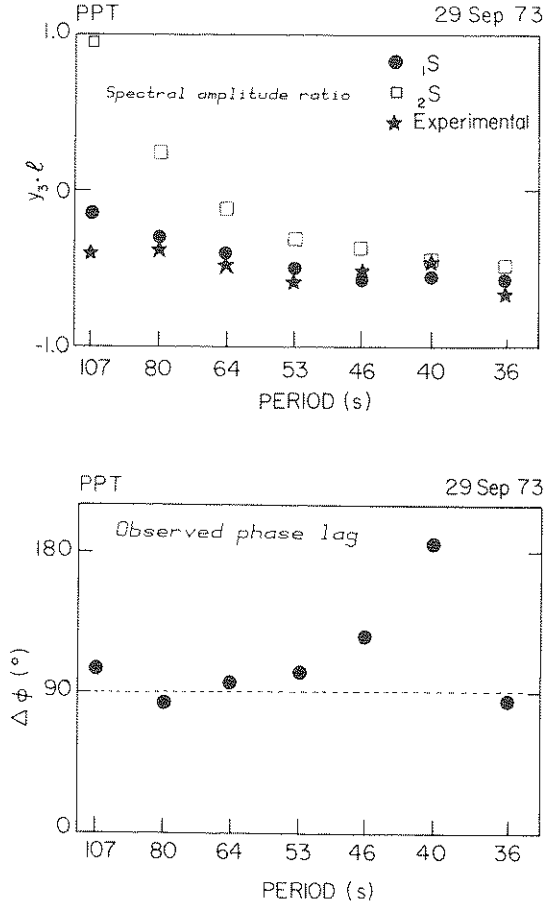

Figure 3. Study of the horizontal to vertical complex aspect ratio of ${}_1R$. Top: amplitude of the aspect ratio observed at PPT following event 1, compared to theoretical values for normal mode branches ${}_1S$ and ${}_2S$, computed in model 1066A. Bottom: observed phase lag between horizontal and vertical components at PPT. Note departure from 90°, in the vicinity of 50 s, suggesting contamination with ${}_2R$. Abscissae linear in frequency.

this lag depends on the particular overtone and, possibly, frequency). If two overtones interfere, they have different aspect ratios, and their vertical components are not in phase, due to propagation to the station with different phase velocities (and possibly, for complex source geometry, different initial phases). There results an essentially random phase relationship between the vertical and radial components of the resulting seismic displacement.

In Fig. 3, we show the results of the investigation of the amplitude and phase relationship of the vertical and radial components of the seismic motion in the 4.84–4.06 km s^{-1} group velocity window at Papeete, Tahiti, following the 1973 Japan Sea earthquake. The top portion of the figure shows the ratio of the spectral amplitudes, and the bottom one the phase lag, both as functions of frequency. It is clear that between 65 and 100 s, the amplitude ratios match the values predicted by 1066A for ${}_1R$, and the phase lag remains close to the expected 90°. Similarly, at periods less than 40 s, the amplitude ratio and phase lag match the values predicted for either ${}_1R$ or ${}_2R$. On the other hand, between 40 and 60 s, the aspect ratio could agree with either ${}_1R$ or ${}_2R$, but the phase lag becomes close to 180°. This suggests that the observed ${}_1R$ surface wave is contaminated by ${}_2R$ at periods less than 65 s, and probably disappears completely below 40 s.

In view of these results, we decided to restrict our dispersion studies to periods greater than 70 s, where ${}_1R$ can be considered non-contaminated. This result is further confirmed by theoretical investigations of the excitation of the normal mode overtones ${}_1S$ and ${}_2S$ in this range of frequencies (Okal 1979b), but we must keep in mind that the 70 s bound on non-contaminated ${}_1R$ could be somewhat structure dependent.

4 Phase velocity investigations

4.1 TECHNIQUE

For the retrieval of phase velocity information, we have chosen to rely exclusively on methods eliminating the need for a complete knowledge of the seismic source. One such method is the so-called two-station method, which was described by Toksöz & Ben-Menahem (1963), and whose advantages have been discussed in detail in Paper I. After digitization of the records at a 2 s sample rate, and Fourier analysing, the phase velocity is retrieved through the classic formula:

$$c(T) = (\Delta_2 - \Delta_1) / \{t_2 - t_1 + T \cdot [(\phi_1 - \phi_2)/2\pi + N]\} ,$$

where Δ_1 and Δ_2 are the distances to the two stations, ϕ_1 and ϕ_2 the spectral phases, t_1 and t_2 the times at the start of the digitization windows, and N a suitable integer. When the two stations involved lie within a few degrees of a common great circle with the epicentre, errors due to source geometry become negligible as compared to $(\phi_1 - \phi_2)$, and in any case errors due to source time function cancel out exactly. The precision of the method is difficult to assess (Mitchell & Yu 1980), and has often been taken as resulting from uncertainties equal to twice the digitizing interval. For typical paths of 3000 km or more, that translates into ± 0.04 km s^{-1}.

Because of the general paucity of data for ${}_1R$, we were able to identify only five two-station paths: LUB–ARE (1973 event), TBI–AFI (1977 event), COL–AAM and PPT–LPA (1978 Izu event) and TPT–RKT (1978 Kuriles event). Additionally, in the case of the 1977 Argentina and 1978 Izu-Bonin earthquakes, we used arrays of n stations (located too close to each other to allow use of the standard two-station method), and obtained the phase velocity through the following spatial filtering procedure: at each frequency, and for a number of trial values of the phase velocity, we phase-equalize the spectrum of each signal to a common epicentral distance (taken as that of the centroid of the array), and stack the

Table 3. (a) Phase velocities obtained by the two-station method.

Event	Path	Phase Velocity (km/s) at period (s)				
		73.1	78.8	85.3	93.1	102.4
1	LUB-ARE	5.34	5.39	5.53	5.67	5.82
2	COL-AAM	5.43	5.54	5.59	*	*
2	PPT-LPA	5.22	5.28	5.42	5.62	5.73
3	TBI-AFT	*	5.49	5.53	5.71	5.87
6	IPT-RKT	5.23	5.38	5.54	5.76	5.95

* No sufficient energy in the record at this period.

Table 3. (b) Phase velocities obtained by spatial filtering.

Event	Region	Phase Velocity (km/s) at period (s)				
		73.1	78.8	85.3	93.1	102.4
2	US	5.45	5.53	5.62	5.70	*
3	Southwest Asia	5.28	5.36	5.54	5.63	5.72

* No sufficient energy in the record at this period.

Table 3. (c) Theoretical phase velocities for a variety of models.

Model	Phase velocities (km/s) at periods (s)								
	70	75	80	85	90	95	100	105	110
MYLT20	5.19	5.28	5.37	5.49	5.55	5.64	5.74	5.83	5.92
MY2050	5.21	5.30	5.39	5.48	5.57	5.67	5.77	5.86	5.95
MY50100	5.22	5.31	5.40	5.50	5.59	5.69	5.78	5.88	5.96
MYGT100	5.23	5.33	5.42	5.52	5.62	5.72	5.82	5.91	6.01
MD19	5.14	5.24	5.33	5.43	5.54	5.64	5.77	5.86	5.93
TJ0	5.10	5.28	5.26	5.34	5.43	5.51	5.60	5.69	5.78
TJC	5.44	5.53	5.62	5.72	5.80	5.90	6.01	6.08	6.17
TJ1	5.32	5.41	5.50	5.59	5.68	5.77	5.87	5.96	6.05
TJ2	5.21	5.30	5.39	5.49	5.58	5.67	5.77	5.86	5.96
TJ3	5.38	5.47	5.56	5.65	5.74	5.84	5.93	6.02	6.11
TJ4	5.12	5.20	5.29	5.38	5.47	5.56	5.65	5.74	5.83

resulting n signals. We select the value of the phase velocity maximizing the spectral amplitude of the stacked signal. It is clear that the standard two-station method represents an analytical solution to this problem for the case of $n = 2$. In the case of more stations, the problem becomes over-determined, and our approach provides a best-fitting solution. We use the following stations: COL, LON, COR, MSO, AAM, DAL, SHA (event 2) in the US, and TAB, SHI, KBL, QUE, NDI (event 3) in south-west Asia.

Results of the phase velocity studies are given in Table 3, and plotted in Fig. 4. The layout of this figure is similar to that used in Paper I for fundamental Rayleigh waves at longer periods: for each of the Fourier-transform periods, the vertical scale has been shifted in order to eliminate the average dispersion and enhance the regional characteristics.

4.2 INTERPRETATION OF OCEANIC DATA

The oceanic lithosphere has been the subject of many detailed seismic investigations, in particular through the use of fundamental surface waves (Leeds *et al.* 1974; Leeds 1975; Forsyth 1975; Yu & Mitchell 1979), and there exists a number of models for its structure, as a function of the age of the plate, which all emphasize a thickening of the lithosphere at the expense of the asthenosphere with increasing age. Most of this information was obtained by age regionalization of paths criss-crossing the Pacific. Using local dispersion as recorded over the French Polynesian array, Okal & Talandier (1980) showed that models derived from age regionalization do indeed predict correct values for fundamental Rayleigh

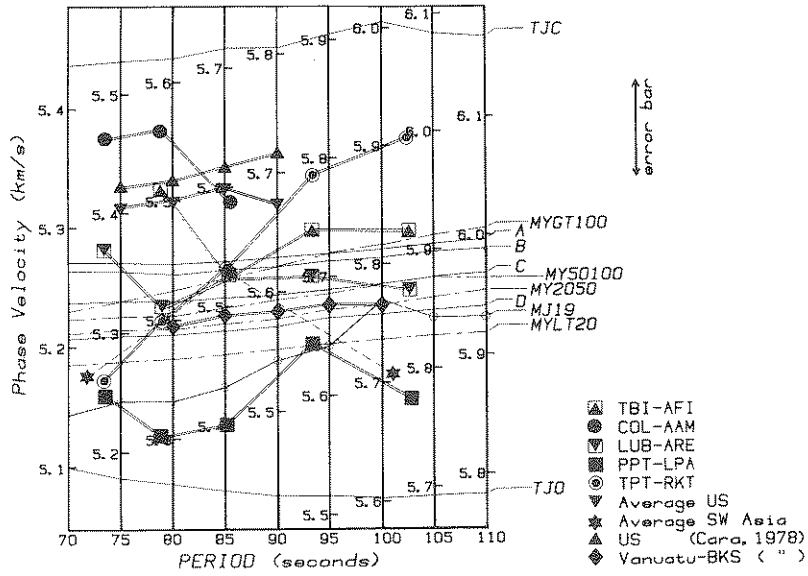

Figure 4. Dispersion of phase velocity of ${}_1R$. At each period, the vertical scale has been offset to enhance clarity (see Paper I). Theoretical values from oceanic models, as well as models TJ0 and TJC, are shown as light lines, and identified at right. Data obtained in this study (and from Cara 1978) are identified with symbols. An estimate of the error bars is also given; note, however, that error bars are about the double for the TPT–RKT path.

dispersion. More recently, Montagner & Jobert (1981) reported lateral variations in fundamental Rayleigh dispersion within the oceanic plates up to periods of 300 s, and proposed a model involving an increase in the depth of the floor of the asthenosphere in the immediate vicinity of the ridge.

In order to interpret our data in the framework of these previous studies, we selected a number of published oceanic models, and computed theoretical dispersion curves for these models, using normal mode formalism. The models include the four models A, B, C, D used in Paper I and originally derived from Leeds' (1975) study, and the four models derived by Mitchell & Yu (1980) from inversion of fundamental Rayleigh waves, which we will call MYLT20, MY2050, MY50100 and MYGT100, after the four ranges of lithospheric age to which they relate. An attenuation correction to the dispersion (Liu, Anderson & Kanamori 1976) was included in the case of the MY models (but not of the Leeds models, derived for a purely elastic earth), to allow direct comparison of our data (uncorrected for attenuation) with the theoretical values. This correction was obtained from the classic formula (Kanamori & Anderson 1977):

$$\Delta C(\omega) = C(\omega) \cdot \ln(\omega/\omega_r)/\pi Q(\omega),$$

using an average oceanic Q model based on Anderson & Hart's (1978) model SL2, and taking $\omega_r = 2\pi$.

Phase velocity curves for these various theoretical models are included in Fig. 4, and listed in Table 3(c). The only purely oceanic paths available in our dataset are TBI–AFI and TPT–RKT. A magnetic anomaly age of 65 Myr can be estimated for the Pacific lithosphere in the vicinity of Tubuai Island (TBI), and AFI sits on lithosphere older than 100 Myr (Jordan 1981). The dispersion along TBI–AFI should therefore be representative of model B (80–135 Myr) or intermediate between MY50100 and MYGT100. Although our observed

values are slightly higher (an average of 0.04 km s^{-1}), the agreement can be considered good, especially in view of our estimated error bars. We have also drawn in Fig. 4 the dispersion values obtained by Cara (1978) along the path Vanuatu–BKS, whose average age is about 50 Myr. These values agree very well with the appropriate MY models, and are about 0.06 km s^{-1} slower than along the older path TBI–AFI.

In the case of the path TPT–RKT, the situation is somewhat more complex, since this path follows the Tuamotu archipelago plateau. In this part of the Pacific, the plateau is a major tectonic feature, presumably of hotspot origin, but its precise genesis is unclear. In their study of fundamental Rayleigh dispersion in the area, Okal & Talandier (1980) reported that phase velocities along this path were anomalously high, even considering the reduced thickness of the water layer accompanying the shallower bathymetry. Thus, in interpreting our data along this path, it must be kept in mind that it is not fully representative of the adjoining lithosphere, whose age would be about 35–60 Myr. Bearing in mind that these data also have larger error bars (± 0.08 km s^{-1}) due to the shorter distance between the two stations (only 1500 km), our results indicate that the $_1R$ dispersion along TPT–RKT may be slightly faster than along TBI–AFI, a path slightly but systematically older in lithospheric age, in agreement with Okal & Talandier's (1980) observations for fundamental Rayleigh waves. Unfortunately, because of the limited amount of dispersion data available along the Tuamotu chain, it is not feasible to invert these results formally into a structure for the chain.

Finally, the path PPT–LPA, which includes a small portion (15 per cent) in the continent of South America, is the slowest obtained in the phase velocity study. This path travels from Tahiti (where the lithosphere is about 65 Myr) across the youngest parts of the Pacific plate, the Easter Island triple junction, along the Challenger Fracture Zone and the Chile Ridge, thus sampling a long segment of very young oceanic lithosphere, whose contribution is

Table 4. (a) Group velocities obtained in this study.

Event–station path	Measured group velocities (km/s) at periods (s)								
	70	75	80	85	90	95	100	105	110
1–AAE$_2$	4.50	4.49	4.48	4.47	4.47	4.47	4.47	*	4.59
1–GRM^2	4.45	4.43	4.40	4.37	4.35	4.39	4.51	4.63	4.64
1–NAI$_2$	4.50	4.51	4.50	4.50	4.49	4.49	4.49	4.50	4.51
1–OBN^2	4.56	4.55	4.53	4.53	4.53	4.53	4.50	4.41	4.48
1–PAS	4.52	4.49	4.46	4.46	4.45	4.45	4.46	4.49	4.54
1–PPT	4.35	4.33	4.32	4.32	4.33	4.35	4.31	4.55	4.57
1–TPT	4.37	4.35	4.34	4.33	4.34	4.35	4.40	4.52	4.56
1–WEL	4.35	4.34	4.34	4.35	4.37	4.44	*	*	*
2–AAE	4.38	4.37	4.37	4.38	4.39	4.38	*	*	*
2–COR	4.33	4.31	*	*	4.39	4.51	4.58	4.63	4.65
2–LON	4.33	4.33	4.32	4.32	4.33	4.35	4.38	4.43	4.44
2–LPA	4.32	4.31	4.31	4.30	4.30	*	*	*	*
2–LPB	4.29	4.29	4.29	4.30	4.31	4.41	4.43	4.44	*
2–NAI	4.36	4.41	4.45	4.46	4.45	*	*	*	*
2–PAS	*	4.51	4.51	4.44	4.44	4.45	4.48	4.52	4.55
2–PPT	*	*	4.26	4.31	4.34	4.36	4.36	*	*
2–WEL	4.35	4.34	4.34	4.35	4.37	4.44	*	*	*
3–AFI	4.42	4.39	4.38	4.37	4.37	4.38	4.41	4.44	4.48
3–ATU	4.59	4.58	4.56	4.54	4.54	4.54	4.55	4.57	4.59
3–BEC	4.65	4.67	4.67	4.64	4.61	4.60	4.62	4.67	4.71
3–CTA	4.48	4.47	4.46	4.46	4.45	4.45	4.47	4.51	*
3–GRM	4.44	4.44	4.44	4.45	4.46	4.48	4.52	4.56	4.60
3–KEV	4.44	4.41	4.38	4.37	4.36	4.38	4.45	*	*
3–NAI	4.47	4.46	4.45	4.45	4.45	4.47	4.50	4.56	4.60
3–SHI	4.54	4.52	4.50	4.47	4.45	4.44	4.45	4.47	4.52
3–TAB	4.49	4.46	4.46	4.46	4.48	4.52	4.56	4.59	4.60
3–TAU	4.55	4.49	4.44	4.41	4.39	4.38	4.37	4.37	4.37
3–TBI	4.39	4.36	4.34	4.33	4.33	4.33	4.35	4.38	4.40
3–WIN	4.38	4.37	4.36	4.36	4.36	4.39	4.42	4.45	4.48
4–PPT	4.38	4.37	4.36	4.35	4.35	4.37	4.38	*	*
4–TPT	4.39	4.37	4.36	4.35	4.35	4.36	4.38	*	*
5–TPT	4.38	4.36	4.34	4.32	4.33	4.33	4.35	4.38	*

* No sufficient energy in the record at this period.

Table 4. (b) Ultra-long period ${}_1R$ group velocities obtained from IDA data and for model 1066A.

Model or event–station path	Group velocity (km/s) at period (s)							
	150	165	180	195	210	225	240	255
1066A	5.22	5.42	5.58	5.67	5.73	5.80	5.83	5.90
$2\text{–}BDF_2$	5.11	5.41	5.49	5.57	5.74	5.92	5.86	*
$2\text{–}SUR_2$	5.38	5.57	5.64	5.66	5.74	5.79	5.84	5.87

* No sufficient energy in the record at this period.

Table 4. (c) Theoretical group velocities for a variety of models.

Model	Group velocities (km/s) at periods (s)								
	70	75	80	85	90	95	100	105	110
MYLT20	4.17	4.19	4.22	4.24	4.27	4.30	4.33	4.38	4.42
MY2050	4.22	4.22	4.24	4.26	4.27	4.31	4.34	4.38	4.44
MY50100	4.22	4.22	4.24	4.26	4.28	4.32	4.35	4.40	4.46
MYGT100	4.17	4.18	4.21	4.24	4.27	4.31	4.36	4.42	4.48
MJ19	4.14	4.13	4.13	4.14	4.16	4.19	4.25	4.31	4.39
TJ0	4.18	4.19	4.20	4.21	4.23	4.24	4.25	4.28	4.31
TJC	4.36	4.39	4.42	4.47	4.51	4.56	4.62	4.67	4.74
TJ1	4.33	4.34	4.36	4.38	4.40	4.42	4.47	4.50	4.56
TJ2	4.22	4.22	4.23	4.25	4.27	4.31	4.35	4.40	4.46
TJ3	4.38	4.40	4.41	4.43	4.45	4.48	4.53	4.56	4.63
TJ4	4.15	4.15	4.17	4.19	4.21	4.24	4.28	4.32	4.37

responsible for the very slow velocities observed. We have compared our results to ${}_1R$ dispersion curves computed from Montagner & Jobert's (1981) model for oceanic lithosphere with an average age of 19 Myr, shown as MJ19 in Fig. 4, and listed in Table 4. Our results are in excellent agreement with this model despite the uncertainties associated with age averaging and with the continental fraction of the path, greater than in these authors' study.

In conclusion to this paragraph, our oceanic phase velocity studies show that there exist differences in ${}_1R$ dispersion in parts of the ocean of different ages: the range of these variations, on the order of 0.12 km s^{-1}, is comparable to that for the ultra-long period fundamental Rayleigh waves studied in Paper I, although no significant decrease of this figure is observed with increasing period, as was then the case. Additionally, we find that ${}_1R$ dispersion is correctly modelled by the available oceanic structures, derived from fundamental data.

4.3 INTERPRETATION OF CONTINENTAL AND TRENCH DATA

Our phase velocity continental data consists of two two-station paths (COL–AAM and LUB–ARE), and data from two regional array studies: US stations for the 1978 Izu-Bonin event, and south-west Asian stations for the 1977 event. The path COL–AAM is mostly in the Canadian shield, whereas the regional US study covers a more heterogeneous area. It is not surprising therefore that COL–AAM should on the average be slightly faster than the average US dispersion, although the difference (0.04 km s^{-1}) is within error bars. Furthermore, our results are in excellent agreement with Cara's (1978), obtained by a similar method from a shallow earthquake in the Vanuatu Islands. The two paths involving a highly tectonic structure (LUB–ARE across the Central and South American subduction zones; and the south-west Asia area, covering Iran and Pakistan) are significantly slower than the paths in the US, by an average of 0.15 km s^{-1}. Furthermore, these paths have phase velocities falling within the range of oceanic ones.

5 Group velocity measurements

5.1 TECHNIQUE

Group velocity measurements were taken over 34 paths, most of which shown in Fig. 2. After digitizing with a 2 s rate, the instrumental response was removed, and a variable filtering technique applied. Details of this technique can be found in Landisman, Dziewonski & Satô (1969), and are reviewed by Pilant (1979). We use central filtering frequencies corresponding to 5 s increments in period from 70 to 110 s. Data were rejected when the spectral amplitude at the frequency involved (before removal of the instrument response) was found to fall below one-half its maximum value for each record over the range of study (shown as * in Table 4). We make use of a Gaussian filter with a parameter $\alpha = 15$ in the notation of Dziewonski, Bloch & Landisman (1969). In our particular case, and because the focal mechanisms involved in the deep subduction events are vertical dip-slips, we did not apply any source group delay corrections, since the source phase is independent of frequency. Moment rate source functions departing significantly from a delta-function could also create a source delay term. For this reason, we specifically rejected records of the 1978 Kuriles event, which may have had a complex rupture history lasting up to 70 s (P. G. Silver 1971 private communication). In the case of event 1, Koyama (1978) has shown that the source duration may be as long as 30 s. At the average distance of 11 000 km, this results in an error of ± 0.025 km s^{-1}. The other events, whose moment is smaller by one order of magnitude, would contribute a smaller term. The intrinsic precision involved in such a method is also difficult to assess; based on discussions by Der, Massé & Landisman (1970) and Yu & Mitchell (1979), and on an average epicentral distance of 11 000 km, we obtain a figure of ± 0.025 km s^{-1}, which when combined with the source error yields a total estimate of ± 0.05 km s^{-1}.

Results are listed in Table 4 and presented in Fig. 5. One important aspect of these results is their excellent repeatability, demonstrated by the additional data obtained in Polynesia from the smaller Japanese events numbers 4 and 5. The agreement between values obtained from both large and small, whose moments differ by more than one order of magnitude, confirms *a posteriori* the lack of influence of source group delay times for the major events.

5.2 ULTRA-LONG PERIOD DATA

Fig. 6 presents results of the investigation of ${}_1R$ dispersion at periods ranging from 150 to 260 s, as obtained from records of ${}_1R_2$ at the IDA stations BDF and SUR. It was not possible to carry this investigation to longer periods because of the coupling of ${}_1R$ with a core-boundary Stoneley mode around 300 s. The precision of such data, governed by the 20 s sampling rate used at IDA stations in 1978, is about 0.07 km s^{-1}. Within these error bars, it is clear that our data, believed to be the first direct measurement of Rayleigh overtone group velocities at these frequencies, agree very well with 1066A. At the only periods (150–180 s) where the difference between the two paths may have significance, the BDF path is slightly slower than the SUR one.

5.3 INTERPRETATION OF OCEANIC DATA

As in the case of phase velocities, we start by analysing our data over pure oceanic paths, for which theoretical models are available. In Fig. 5, we have plotted as dotted lines the range of variation of group velocities for the following oceanic models: A, B, C, D, the MY models and MJ19. Attenuation corrections, on the order of -0.05 km s^{-1}, were included in the case

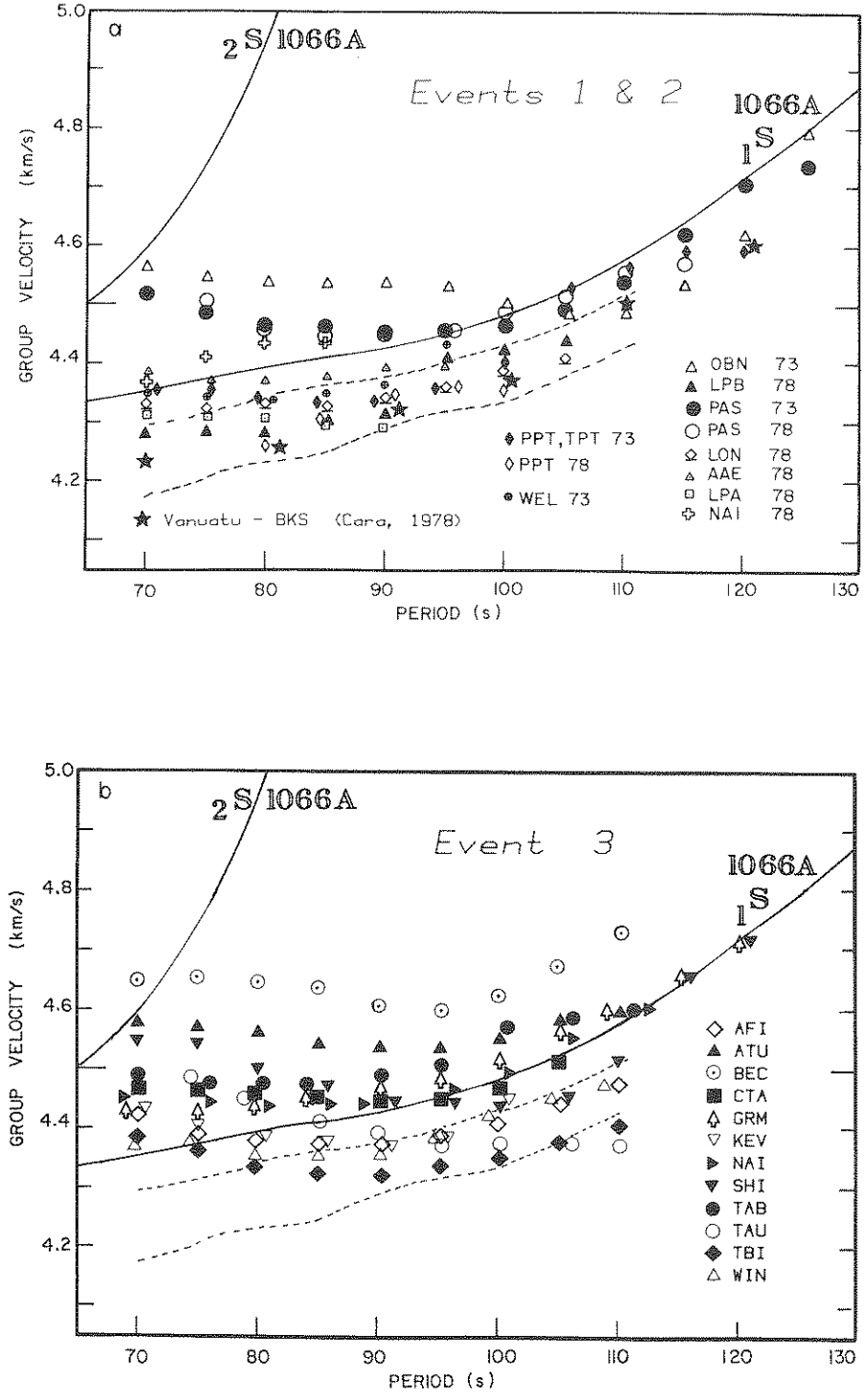

Figure 5. (a) Group velocity data for events 1 and 2. The solid lines represent theoretical values for model 1066A; the dashed lines represent the range of variation of theoretical velocities for the oceanic models. Various symbols are used for the different paths (key at right). Occasionally, symbols were displaced slightly along a horizontal line, to enhance clarity. (b) Same as (a) for event 3.

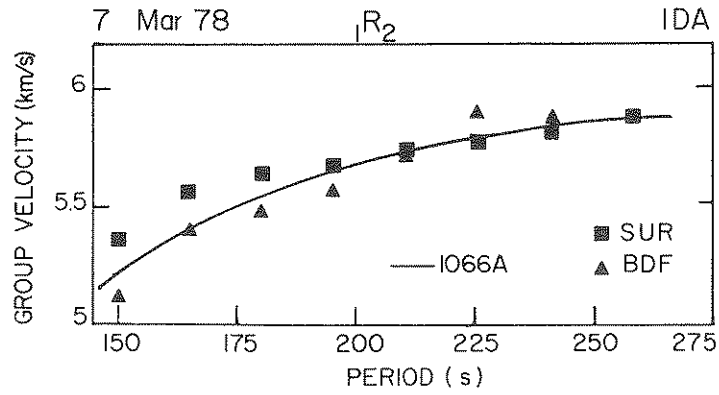

Figure 6. Group velocity data obtained from IDA records of event 2 at ultra-long periods, compared to theoretical values for model 1066A.

of the MY models (neither 1066A, Leeds' models nor MJ19 include attenuation corrections, so direct comparison with the data is possible). The most important feature immediately observed on these model curves is that the scatter of oceanic group velocities with lithospheric age (about 0.10 km s^{-1} above 85 s) is slightly less intense than for phase velocities (about 0.12 km s^{-1}). In general, this is a reflection of the fact that the group velocity partial derivative with respect to shear velocity, has a more irregular behaviour than its phase velocity counterpart (see Fig. 7), resulting in a less efficient integration of the change in structure with age.

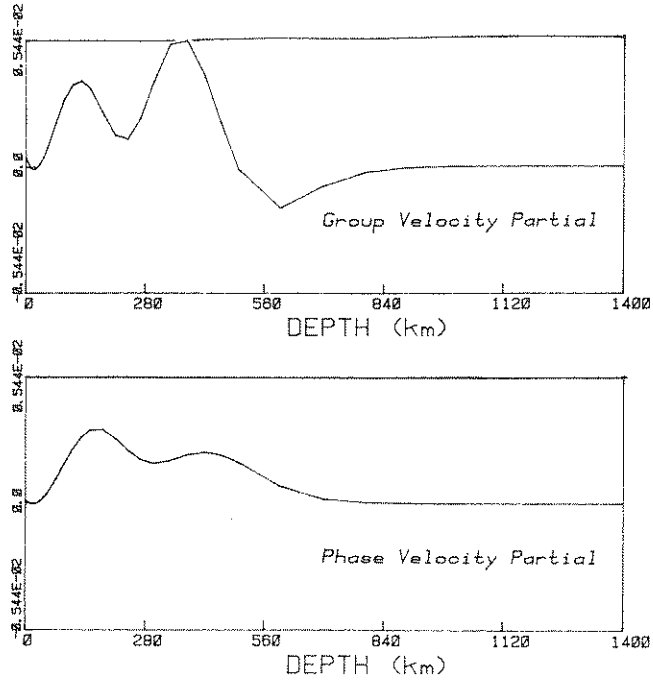

Figure 7. Partial derivative of phase and group velocity with respect to shear velocity, computed for model 1066A, and for $_1S_{90}$, (T = 80 s). Units are km^{-1} (Aki & Richards 1980, p. 292). These partials are derived from normal mode theory, and as such, taken at constant wavenumber. Group velocity partials are obtained by adapating Rodi *et al.*'s (1975) formalism to constant wavenumber.

Our experimental data along oceanic paths confirm this pattern: Although some of our slowest values are found along Argentina–TBI and Japan–LPA, which sample a large fraction of young lithosphere (see discussion above), they are not significantly slower than paths sampling older lithosphere, such as Japan–PPT, or Japan–WEL, and are very comparable to Cara's (1978) observations along the path Vanuatu–BKS.

5.4 CONTINENTAL DATA

The only purely continental path along which we have group velocity data is Japan Sea–OBN, across Siberia. This path is significantly faster than all oceanic paths and than paths with both continental and oceanic sections. Additionally, Argentine–BEC, across the Brazilian shield, and the Caribbean arc is also among our fastest paths.

In order to interpret our data pertaining to mixed paths, we use the same approach as in Paper I. We split each path into oceanic and continental sections, and further distinguish between shield areas (S) and mountainous (or tectonic) continental provinces (M), using the same regionalization map as in Paper I. We include a 'T' region characteristic of trenches, island arcs and subduction zones. Following the scheme developed in Paper I, we constrain the oceanic velocities and solve only for the S, M and T models. This procedure restricts the number of unknowns, and adds stability to the process. In doing so, and because of the relatively small variation of observed group velocity with age in the ocean (as opposed to the situation for phase velocities), we combine the oceanic regions A, B, C, D identified in Paper I, and use only one known oceanic model, for which we take a dispersion obtained by averaging the eight theoretical oceanic group velocity models discussed above. We also restrict our dataset to 10 paths, involving significant continental contributions, eliminating paths travelling mostly in the ocean, since errors associated with them bring instability in the inversion. Paths used in the inversion, together with relevant geographic data are listed in Table 5(a), and the resulting values for regions S, M, T are given in Table 5(b). Standard deviations computed for these results were found to be on the order of 0.15 km s^{-1}. In order to test the validity of our simplifying assumptions introduced in this scheme, we conducted a number of studies involving a larger number of paths, and an intrinsic regionalization of the ocean. Although this occasionally created more intrinsic oceanic heterogeneity than warranted by our observations, results for continental models were significantly stable,

Table 5. (a) Regionalization of paths use in inversion for continental group velocities.

Event–station path	Percentage of path in regions			
	Oceanic	Shield	Mountain	Trench
1–PAS	42	0	21	37
1–WEL	24	0	10	67
1–AAE$_2$	57	10	23	11
1–NAI$_2$	63	8	17	12
2–AAE^2	23	18	55	5
2–NAI	35	13	48	4
3–ATU	17	63	0	21
3–NAI	57	30	9	4
3–TAB	18	57	14	11
3–SHI	31	49	17	3

Table 5. (b) Results of inversion for group velocities in regions S, M, T obtained from 10 paths, with oceanic velocities constrained.

Region	Group velocities (km/s) at periods (s)								
	70	75	80	85	90	95	100	105	110
S	4.67	4.63	4.60	4.58	4.58	4.58	4.57	4.60	4.61
M	4.33	4.41	4.45	4.47	4.46	4.41	4.54	4.46	4.59
T	4.41	4.44	4.43	4.43	4.46	4.53	4.57	4.57	4.60

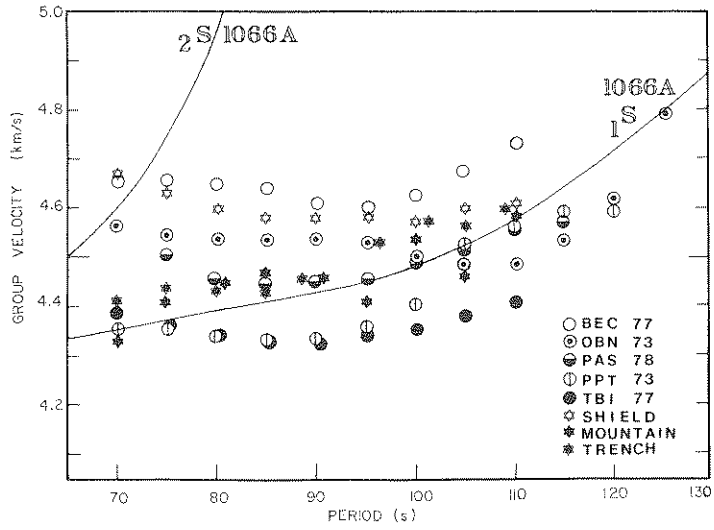

Figure 8. Result of inversion for continental group velocities, plotted with a sample of the data from Fig. 5.

usually within the range of error bars accompanying our data (0.05 km s^{-1}) and *a fortiori* within one standard deviation of our solutions (0.15 km s^{-1}).

The resulting dispersion values in regions S, M and T are plotted in Fig. 8, along with a sample of the data presented in Fig. 5. It is clear at first sight that average continental velocities for models S and M are faster than their oceanic counterparts, by approximately 0.20–0.25 km s^{-1}. Furthermore, the shield velocities (S) are found in good agreement (0.03–0.10 km s^{-1}) with observed data on the paths Japan–OBN and Argentina–BEC, which were not included in the inversion dataset. Finally, velocities for tectonic areas (M) are about 0.12–0.15 km s^{-1} slower than for shields. The generally larger scatter of group velocities at periods close to 70 s may be an artefact of an earlier start of the contamination with $_2R$ in continental shield areas.

Finally, the values obtained for model (T), representative of trenches, island arcs and subduction zones are comparable to model (M), and faster than for the MY oceanic models. In particular, velocities along trenches, such as the Aleutian area, are responsible for the relatively fast path Japan–PAS. As pointed out by Jordan (1981), such results must be treated with caution, since the areas regrouped under this label may have widely varying structure; indeed this geographic category has sometimes been referred to as the 'waste basket' of regionalization, and the model created by inversion might therefore not have much significance. In particular, from the partial derivative data shown in Fig. 7, one would expect the presence of a cold slab at 350 km to boost group velocities, but on the other hand, the simultaneous presence of a marginal sea at 150 km would act in the opposite direction.

6 Discussion

Both our phase and group velocity results have shown that oceanic models, as obtained by a variety of authors from fundamental Rayleigh wave studies, correctly predict dispersion along purely oceanic paths. The range of variation of velocities with age, on the order of 0.12 km s^{-1} for phase velocities and only 0.10 km s^{-1} for group velocities, agree with the

various structural models expressing the thickening of the lithosphere. Our PPT–LPA two-station path supports the extremely slow dispersion argued for by Montagner & Jobert (1981) and taken to represent a deepening of the asthenospheric channel in the immediate vicinity of the East Pacific Ridge.

The most important aspects of this study concerns the relative dispersion in oceanic versus continental areas: we have shown that continents are usually faster than oceans, about 0.20 km s^{-1} on the average, both for phase and group velocities. In this respect, our results are apparently different from those in Paper I, where we had obtained ultra-long period fundamental phase velocities over continents comparable to those over the oldest parts of the oceans. However, as we will show, they do not require deep lateral heterogeneity.

In order to investigate the possible extent of deep lateral heterogeneity between oceans and continents, we have computed theoretical dispersion curves for two models derived from profiles sketched by Jordan (1975), and referred to in Paper I as TJ0 (oceans) and TJC (continents). These profiles exhibit strong heterogeneity down to 675 km, with continental

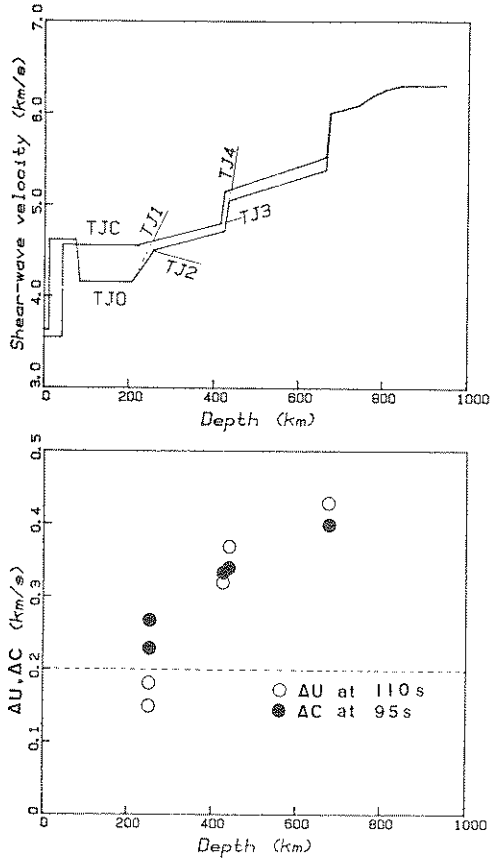

Figure 9. Influence of maximum depth of structural heterogeneities between continents and oceans on dispersion of ${}_1R$. Top: shear-wave velocity profiles for a number of models. The solid lines are Jordan's (1975) sketched continental (TJC) and oceanic (TJ0) profiles. In the areas where they differ from them, the intermediate models TJ1–TJ4 are shown by dashed lines, and identified along oblique lines (see text for details). Bottom: Difference in ${}_1R$ continental versus oceanic phase velocity at 95 s, and group velocity at 110 s, for these various models, plotted as a function of the depth of maximum heterogeneity in their structure. The dashed line represents our average data (with a standard deviation of ± 0.05 km s^{-1} at this period), and suggests a maximum depth of 250 km.

shear wave velocities on the average 0.15 km s^{-1} faster than oceanic ones below the asthenospheric channel (see Fig. 9). Although these are not models designed to fit a definite set of body- and surface-wave data, they provide a useful example of what substantial lateral heterogeneity between continents and oceans could be, if it extended to great depths; it is in this context that we will make use of these models. As shown in Fig. 4, they predict differences in phase velocity of the order of 0.40 km s^{-1}, all across our ranges of frequencies. This is twice as much as we observe. Similarly, they predict differences in group velocity increasing from 0.18 km s^{-1} at 70 s to 0.43 km s^{-1} at 110 s (this increase is due to a strong increase with period of the partial derivative with respect to shear velocity taken at 500–600 km). Although this would agree with our observed data at the high-frequency end of the spectrum, our group velocities around 100–110 s are separated by only 0.20 km s^{-1} at the most.

Because of the relatively small amount of data points which we have gathered we chose not to try to invert our dataset formally into a structural model for continents. Rather, we have perturbed the oceanic and continental models, so as to constrain the depth of lateral heterogeneities to a variable figure starting with the two models TJ0 and TJC, and moving the depth of homogeneity up to the bottom of the asthenosphere (250 km) in several steps. Details of these models, presented in Fig. 9, are as follows: model TJ0, featuring a well-developed low-velocity zone is representative of a young ocean; model TJC, with no LVZ, would apply to a shield area, and differ down to 675 km. Additionally, we create four intermediate models: TJ4 and TJ2 are oceanic models similar to TJ0, but rejoining TJC at 450 and 250 km, respectively, while TJ3 and TJ1 are continental models smilar to TJC, but rejoining TJ0 at the same depths. Because these are only theoretical models, we pay no attention to their absolute dispersion curves; rather, we concentrate on the differences in dispersion between them. As shown in Tables 3(c) and 4(c), and in Fig. 9, two models with structural differences down to 250 km such as TJ0 and TJ1 (or TJC and TJ2) are expected to feature an offset of about 0.25 km s^{-1} in phase velocity, and 0.22 km s^{-1} in group velocity at a period of 95 s. If we allow substantial structural differences to reach 430 km, a comparison between TJ0 and TJ3 (or between TJC and TJ4) boosts these figures to 0.33 and 0.29 km s^{-1}. Finally, at 675 km, these figures are (directly from TJ0 and TJC) 0.39 and 0.32 km s^{-1}. Surprisingly enough, because of a region of negative group velocity partial derivatives around 400 km, the removal of heterogeneities in this range has little effect on the scatter of group velocities around 70–80 s, and may actually work to increase it. The bottom part of Fig. 9 provides a graphic solution to the problem of the depth of strong continent versus ocean structural heterogeneities warranted by our data, and yields a figure of about 250 km, in agreement with the results of Paper I.

Finally, it should be noted that the shear wave variation derived for the second harmonic of the heterogeneity from fundamental mode data by Masters *et al.* (1982) at depths of 420–670 km is only 1.7 per cent rms; Fig. 7 shows that the effect of these variations, integrated on depth will only be on the order of 1 per cent or 0.05 km s^{-1}. This is the limit of our precision, and therefore it would be futile to try to use our dataset in an attempt to check their model.

7 Conclusions

The major conclusions of this paper can be summarized as follows:

(1) High-quality dispersion characteristics can be retrieved from individual wavetrains of the first Rayleigh overtone on records of deep subduction zone events, in the period range 70–110 s.

(2) Phase velocity data uphold oceanic models generated from fundamental Rayleigh observations. The range of variation of phase velocity with age is on the order of 0.12 km s^{-1}, a figure compatible, within error bars, with published models, including Montagner & Jobert's (1981) one for very young lithosphere. Phase velocity continental data suggests values about 0.20 km s^{-1} higher, across the frequency range involved.

(3) Group velocities in oceanic areas are generally compatible, within error bars, with values predicted by the same theoretical models, although they exhibit a larger scatter, not significantly correlated with age. Continental velocities obtained through regionalization of impure paths are about 0.20 km s^{-1} higher than average oceanic ones at periods greater than 85 s, and up to 110 s.

(4) This behaviour is not compatible with the existence of substantial lateral heterogeneities at great depths; an experiment involving theoretical models shows that a maximum depth of 250 km for continent versus ocean structural differences can be reconciled with our data.

Acknowledgments

We thank Brian Mitchell for detailed versions of the Mitchell and Yu models, Paul Silver for discussion on the rupture mechanisms of some subduction zone events, and Tom Jordan for a preprint of the Masters *et al.* paper. We are grateful to Oleg Starovoit for the Obninsk records, and to Jacques Talandier for those from the French Polynesian network. Normal mode computations were performed using a program originally written by Ralphe Wiggins. This research was supported by the National Science Foundation, under grants EAR-79-03907 and EAR-81-06106.

References

Aki, K. & Richards, P. G., 1980. *Quantitative Seismology*, Freeman, San Francisco, 932 pp.

Anderson, D. L. & Hart, R. S., 1978. Attenuation models of the Earth, *Phys. Earth planet. Int.*, **16**, 289–306.

Cara, M., 1978. Regional variation of higher Rayleigh mode phase velocities: a spatial filtering method, *Geophys. J. R. astr. Soc.*, **54**, 439–460.

DePaolo, D. J., 1981. Nd isotopic studies: some new perspectives on Earth structure and evolution, *Eos, Trans. Am. Geophys. Un.*, **62**, 137–140.

Der, Z., Massé, R. & Landisman, M., 1970. Effects of observational errors on the resolution of surface waves at intermediate distances, *J. geophys. Res.*, **75**, 3399–3409.

Dziewonski, A. M., 1970. On regional differences in dispersion of surface waves, *Geophys. J. R. astr. Soc.*, **22**, 289–325.

Dziewonski, A. M., Bloch, S. & Landisman, M., 1969. A technique for the analysis of transient seismic signals, *Bull. seism. Soc. Am.*, **59**, 427–444.

Forsyth, D. W., 1975. The early structural evolution and anisotropy of the oceanic upper mantle, *Geophys. J. R. astr. Soc.*, **43**, 103–162.

Furumuto, M. & Fukao, Y., 1976. Seismic moments of great deep shocks, *Phys. Earth planet. Int.*, **11**, 352–357.

Gilbert, F. & Dziewonski, A. M., 1975. An application of normal mode theory to the retrieval of structural parameters and source mechanisms from seismic spectra, *Phil. Trans. R. Soc. A*, **278**, 187–269.

Jordan, T. H., 1975. Lateral heterogeneity and mantle dynamics, *Nature*, **257**, 745–750.

Jordan, T. H., 1978. A procedure for estimating lateral variations from low-frequency eigenspectra data, *Geophys. J. R. astr. Soc.*, **52**, 441–455.

Jordan, T. H., 1979. Structural geology of the Earth's interior, *Proc. natn. Acad. Sci. USA*, **76**, 4192–4200.

Jordan, T. H., 1981. Global tectonic regionalization for seismological data analysis, *Bull. seism. Soc. Am.*, **71**, 1131–1141.

Kanamori, H., 1970. Velocity and Q of mantle waves, *Phys. Earth planet. Int.*, **2**, 259–275.

Kanamori, H. & Anderson, D. L., 1977. Importance of physical dispersion in surface wave and free oscillation problems: review, *Rev. Geophys. Space Phys.*, **15**, 105–112.

Kanamori, H. & Cipar, J. J., 1974. Focal process of the great Chilean Earthquake, May 22, 1960, *Phys. Earth planet. Int.*, **9**, 128–136.

Knopoff, L., 1972. Observation and inversion of surface-wave dispersion, *Tectonophys.*, **13**, 497–519.

Koyama, J., 1978. Seismic moment of the Vladivostok deep-focus earthquake of September 29, 1973 deduced from P waves and mantle Rayleigh waves, *Phys. Earth planet. Int.*, **16**, 307–317.

Landisman, M., Dziewonski, A. M. & Satô, Y., 1969. Recent improvements in the analysis of surface wave observations, *Geophys. J. R. astr. Soc.*, **17**, 369–403.

Leeds, A. R., 1975. Lithospheric thickness in the Western Pacific, *Phys. Earth planet. Int.*, **11**, 61–64.

Leeds, A. R., Kausel, E. G. & Knopoff, L., 1974. Variations of upper mantle structure under the Pacific Ocean, *Science*, **186**, 141–143.

Liu, H.-P., Anderson D. L. & Kanamori, H., 1976. Velocity dispersion due to anelasticity, *Geophys. J. R. astr. Soc.*, **47**, 41–58.

Masters, T. G. & Gilbert, J. F., 1979. Source retrieval from a sparse long-period network, *Eos, Trans. Am. Geophys. Un.*, **60**, 879 (abstract).

Masters, G., Jordan, T. H., Silver, P. G. & Gilbert, F., 1982. Aspherical earth structure from fundamental spheroidal-mode data, *Nature*, **298**, 609–613.

Mitchell, B. J. & Yu, G.-K., 1980. Surface wave velocities, anelasticity corrections, and regionalized velocity models of the Pacific crust and upper mantle, *Geophys. J. R. astr. Soc.*, **63**, 497–514.

Montagner, J.-P. & Jobert, N., 1981. Investigation of upper mantle structure under young regions of the southeast Pacific using long-period Rayleigh waves, *Phys. Earth planet. Int.*, **27**, 206–222.

Nakanishi, I., 1981. Shear velocity and shear attenuation models inverted from the world-wide and pure-path average data of mantle Rayleigh waves ($_0S_{25}$ to $_0S_{80}$) and fundamental spheroidal modes ($_0S_2$ to $_0S_{24}$), *Geophys. J. R. astr. Soc.*, **66**, 83–130.

Nakanishi, I. & Anderson, D. L., 1981. Lateral variations of Rayleigh wave group velocity: spherical harmonic expansion, *Eos, Trans. Am. Geophys. Un.*, **62**, 947 (abstract).

Okal, E. A., 1977. The effect of intrinsic oceanic upper-mantle heterogeneity on regionalization of long-period Rayleigh wave phase velocities, *Geophys. J. R. astr. Soc.*, **49**, 357–370.

Okal, E. A., 1979a. Higher mode Rayleigh waves studied as individual seismic phases, *Earth planet. Sci. Lett.*, **43**, 162–167.

Okal, E. A., 1979b. Phase and group velocities along individual paths for Rayleigh wave overtones, *Eos, Trans. Am. Geophys. Un.*, **60**, 879 (abstract).

Okal, E. A. & Anderson, D. L., 1975. A study of lateral heterogeneities in the upper mantle by multiple *ScS* travel-time residuals, *Geophys. Res. Lett.*, **2**, 313–316.

Okal, E. A. & Talandier, J., 1980. Rayleigh wave phase velocities in French Polynesia, *Geophys. J. R. astr. Soc.*, **63**, 719–733.

Pilant, W. L., 1979. *Elastic Waves in the Earth*, Elsevier, New York, 493 pp.

Poupinet, G., 1979. On the relation between *P*-wave travel time residuals and the age of continental plates, *Earth planet. Sci. Lett.*, **43**, 149–161.

Rodi, W. L., Glover, P., Li, T. M. C. & Alexander, S. S., 1975. A fast accurate method for computing group velocity partial derivatives for Rayleigh and Love waves, *Bull. seism. Soc. Am.*, **65**, 1105–1114.

Romanowicz, B. A., 1979. Seismic structure of the upper mantle beneath the United States by three-dimensional inversion of body wave arrival times, *Geophys. J. R. astr. Soc.*, **57**, 479–506.

Romanowicz, B. A., 1980. A study of large-scale lateral variations of *P* velocity in the upper mantle beneath western Europe, *Geophys. J. R. astr. Soc.*, **63**, 217–232.

Silver, P. G. & Jordan, T. H., 1981. Fundamental spheroidal mode observations of aspherical heterogeneity, *Geophys. J. R. astr. Soc.*, **64**, 605–634.

Sipkin, S. A. & Jordan, T. H., 1976. Lateral heterogeneity in the upper mantle determined from the travel times of multiple *ScS*, *J. geophys. Res.*, **81**, 6307–6331.

Sipkin, S. A. & Jordan, T. H., 1980. Multiple *ScS* in the western Pacific: implications for mantle heterogeneity, *J. geophys. Res.*, **85**, 853–861.

Toksöz, M. N. & Anderson, D. L., 1966. Phase velocities of long-period surface waves and structure of the upper mantle; 1: great-circle Love and Rayleigh wave data, *J. geophys. Res.*, **71**, 1649–1658.

Toksöz, M. N. & Ben-Menahem, A., 1963. Velocities of mantle Love and Rayleigh waves over multiple paths, *Bull. seism. Soc. Am.*, **53**, 741–764.

Tréhu, A. M., Sclater, J. G. & Nabelek, J., 1976. The depth and thickness of the ocean crust and its dependence upon age, *Bull. Soc. géol. Fr. Sér. 7*, **18**, 917–930.

Yu, G.-K. & Mitchell, B. J., 1979. Regionalized shear velocity models of the Pacific upper mantle from observed Love and Rayleigh wave dispersion, *Geophys. J. R. astr. Soc.*, **57**, 311–341.